9-2014

On UAV Robust Nonlinear Control in Presence of Parametric Uncertainties

Vladimir V. Golubev
Embry-Riddle Aeronautical University

William MacKunis
Embry-Riddle Aeronautical University, mackuniw@erau.edu

29th Congress of the International Council of the Aeronautical Sciences
St. Petersburg, Russia; September 7-12, 2014

ON UAV ROBUST NONLINEAR CONTROL IN PRESENCE OF PARAMETRIC UNCERTAINTIES

Vladimir V. Golubev*, William MacKunis**
***Aerospace Engineering, **Engineering Physics**
Florida Center for Advanced Aero Propulsion
Embry-Riddle Aeronautical University
Daytona Beach, FL 32114, USA

Keywords: *Robust Control, LCO, Synthetic-Jet Actuator*

Abstract

We examine a new robust nonlinear flight control technology that employs an array of synthetic-jet micro-actuators embedded in UAV wing design in order to completely eliminate moving parts (such as ailerons) thus greatly enhancing maneuverability required for small fixed-wing air vehicles operating, e.g., in tight urban environments. Estimated fast response times are critical in mitigating gust effects while greatly improving flight stability and control. The new controller design is particularly advantageous for high levels of uncertainty and nonlinearity present both in the unsteady flow-path environment and in the embedded actuator's response. The current work focuses on a benchmark case of flutter control of 2-DOF elastically-mounted airfoil entering limit-cycle oscillations (LCO) due to impinging upstream flow disturbance. Preliminary parametric studies conducted for various SJA excitation amplitudes and frequencies examine the thresholds of the actuator's control authority to produce a desirable impact.

1 Introduction

We address the development of a novel robust flight control system employing a distributed array of zero-net-mass-flux synthetic-jet actuators (SJAs). Due to their small size, ease of operation, and low cost, such micro-actuators may represent promising tools for aircraft tracking control applications. Arrays consisting of several SJAs can be employed to achieve high maneuvering capabilities of an aircraft while possibly eliminating the need for mechanical control surfaces. The benefits of utilizing SJAs on aircraft as opposed to mechanical control surfaces also may include reduced cost and weight, minimal mechanical complexity, and low observability.

Uncertainties inherent in the dynamics of the unsteady fluid-structure interactions [1-2] present significant challenges in the control design. Moreover, the input-output characteristics of each SJA are nonlinear and contain parametric uncertainties [3]. Adaptive and neural network-based techniques may produce effective means of compensating for actuator nonlinearities and uncertainty; however, such techniques require additional computational complexity over purely robust feedback designs. Hence, the minimalism of the controller design in this work is motivated by the desire to develop control methods that are suitable for small UAVs with limited onboard computational capability. In the current research study, the novel robust and above-mentioned control methods is examined and compared for their ability to compensate for parametric uncertainties in SJA dynamics and to achieve highly efficient suppression of limit-cycle

oscillations (LCOs) in the gust-induced flutter conditions and accurate trajectory tracking for small unmanned aircraft.

As a benchmark problem to examine application of the proposed methodology, the current study particularly focuses on a fixed-wing elastically-mounted low-speed airfoil operating in a gusty environment (Fig. 1). We thus consider robust control of the gust-induced LCO as the latter may significantly affect the aerodynamic properties of an aircraft and can be especially problematic for small UAVs.

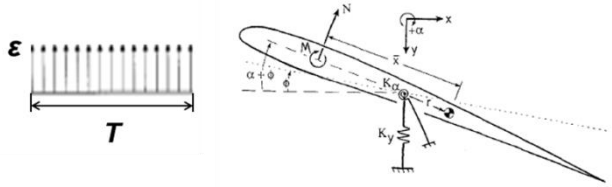

Fig. 1. Sharp-Edge Gust-Airfoil Interaction Model.

The current proof-of-concept analysis employs a reduced-order model, with the representative set of structural parameters selected to provide a realistic model of elastically-mounted UAV wing section.

2 Theoretical Formulation

The equations describing the unsteady response of an elastically-mounted 2-DOF airfoil approximated as a flat plate can be expressed as (e.g., Refs. [4-6]),

$$M_s \ddot{p} + C_s \dot{p} + F(p)p = \begin{bmatrix} -Lift \\ Moment \end{bmatrix} \tag{1}$$

where the coefficients $M_s,\ C_s \in \mathbb{R}^{2\times 2}$ denote the structural mass and damping matrices, $F(p) \in \mathbb{R}^{2\times 2}$ is a nonlinear stiffness matrix, and $p(t) \in \mathbb{R}^2$ denotes the state vector. In Eqn. (1), $p(t)$ is explicitly defined as

$$p = \begin{bmatrix} h \\ \alpha \end{bmatrix} \tag{2}$$

where $h(t),\ \alpha(t) \in \mathbb{R}$ denote the plunging [meters] and pitching [radians] displacements describing the LCO effects. Also in Eqn. (1), the structural linear mass matrix M_s is defined as

$$M_s = \begin{bmatrix} m & S_\alpha \\ S_\alpha & I_\alpha \end{bmatrix} \tag{3}$$

where the parameters $S_\alpha,\ I_\alpha \in \mathbb{R}$ are the static moment and moment of inertia, respectively. The structural linear damping matrix is described as

$$C_s = 2\begin{bmatrix} \zeta_h \sqrt{k_h m} & 0 \\ 0 & \zeta_a \sqrt{k_\alpha I_\alpha} \end{bmatrix} \tag{4}$$

where the parameters $\zeta_h,\ \zeta_\alpha \in \mathbb{R}$ are the damping logarithmic decrements for plunging and pitching, and $m \in \mathbb{R}$ is the mass of the wing, or in this case, a flat plate. The nonlinear stiffness matrix utilized in this study is

$$F(p) = \begin{bmatrix} k_h & 0 \\ 0 & k_\alpha + k_{\alpha^3}\alpha^2 \end{bmatrix} \tag{5}$$

where $k_\alpha,\ k_{\alpha^3} \in \mathbb{R}$ denote structural resistances to pitching (linear and nonlinear) and $k_h \in \mathbb{R}$ is the structural resistance to plunging.

In Eq. (1), the total lift and moment are explicitly defined as

$$\begin{bmatrix} -Lift \\ Moment \end{bmatrix} = \begin{bmatrix} -(L + L_{v_j}) \\ (M + M_{v_j}) \end{bmatrix} = M_a \ddot{p} + C_a \dot{p} + K_a p + L_\eta \eta + B\delta \tag{6}$$

where $\delta = \left[-L_{vj}; M_{vj}\right] \in \mathbb{R}^2$ denote the equivalent control force and moment, respectively due to the virtual surface deflection generated by *j*th SJA, and $L,\ M \in \mathbb{R}$ are the aerodynamic lift and moment due to the 2-DOF motions. In Eq. (6), $\eta \in \mathbb{R}^2$ denotes the aerodynamic state vector that relates the moment and lift to the structural modes. Also in Eqn. (6), the aerodynamic and mode matrices $M_a,\ C_a,\ K_a,\ L_\eta \in \mathbb{R}^{2\times 2}$ are described as

$$M_a = \pi\rho b^2 \begin{bmatrix} -1 & ba \\ ba & -b^2\left(\frac{1}{8} - a^2\right) \end{bmatrix}, \tag{7}$$

$$C_a = \pi\rho b^2 \begin{bmatrix} 0 & -U \\ 0 & -Ub\left(\frac{1}{2} - a\right) \end{bmatrix} + 2\pi\rho Ub\phi(0) \begin{bmatrix} -1 & -b\left(\frac{1}{2} - a\right) \\ b\left(\frac{1}{2} + a\right) & b^2\left(\frac{1}{2} + a\right)\left(\frac{1}{2} - a\right) \end{bmatrix} \tag{8}$$

$$K_a = 2\pi\rho Ub\phi(0) \begin{bmatrix} 0 & -U \\ 0 & b\left(\frac{1}{2} + a\right)U \end{bmatrix} \tag{9}$$

$$L_\eta = 2\pi\rho Ub\begin{bmatrix} a_1 b_1 & a_2 b_2 \\ -b\left(\frac{1}{2}+a\right)a_1 b_1 & -b\left(\frac{1}{2}+a\right)a_2 b_2 \end{bmatrix} \quad (10)$$

where $\phi(0)$ is the Wagner solution function at 0, and the parameters $a_1,\ b_1,\ a_2,\ b_2 \in \mathbb{R}$ are the Wagner coefficients. The aerodynamic state variables are governed by

$$\dot{\eta} = C_\eta \dot{p} + K_\eta p + S_\eta \eta \quad (11)$$

The aerodynamic state matrices in Eqn. (11), $C_\eta,\ K_\eta,\ S_\eta \in \mathbb{R}^{2\times 2}$, are explicitly defined as

$$C_\eta = \frac{U}{b}\begin{bmatrix} -1 & -b\left(\frac{1}{2}-a\right) \\ -1 & -b\left(\frac{1}{2}-a\right) \end{bmatrix} \quad (12)$$

$$K_\eta = \frac{U}{b}\begin{bmatrix} 0 & -U \\ 0 & -U \end{bmatrix} \quad (13)$$

$$S_\eta = \frac{U}{b}\begin{bmatrix} -b_1 & 0 \\ 0 & -b_2 \end{bmatrix} \quad (14)$$

By substituting Eqn. (6) into Eqn. (1) the LCO dynamics can be expressed as

$$M\ddot{p} = -C\dot{p} - Kp + L_\eta \eta + B\delta \quad (15)$$

where $C = C_s - C_a$, $K = F(p) - K_a$ and $M = M_s - M_a$.

2.1 Robust Feedback-Loop Controller

One of the objectives of the current study is to design the control signal $u(t)$ to regulate the plunging and pitching dynamics (i.e. $h(t)$, $\alpha(t)$) to zero. To facilitate the control design, the expression in Eqn. (15) is rewritten as

$$M\ddot{p} = g(h,\alpha,\eta) + Bu \quad (16)$$

where $g(h,\alpha,\eta)$ is an unknown, unmeasurable auxiliary function. To quantify the control objective, a regulation error $e_1(t) \in \mathbb{R}^2$ and auxiliary tracking error variables $e_2(t),\ r(t) \in \mathbb{R}^2$ are defined as

$$e_1 = p - p_d \quad (17)$$

$$e_2 = \dot{e}_1 + \alpha_1 e_1 \quad (18)$$

$$r = \dot{e}_2 + \alpha_2 e_2 \quad (19)$$

where $\alpha_1,\ \alpha_2 > 0 \in \mathbb{R}^+$ are user-defined control gains, and the desired plunging and pitching states $p_d = 0$ for the plunging and pitching suppression objective. To facilitate the following analysis, Eqn. (19) is pre-multiplied by M and the time derivative is calculated as

$$M\dot{r} = M\ddot{e}_2 + \alpha_2 M\dot{e}_2. \quad (20)$$

After using Eqns. (16) - (19), the open-loop error dynamics is obtained as

$$M\dot{r} = \tilde{N} + N_d + B\dot{u} - e_2 \quad (21)$$

where the unknown, unmeasurable auxiliary functions $\tilde{N}(e_1,e_2,r)$, $N_d(p_d,\ddot{p}_d) \in \mathbb{R}^2$ are defined as

$$\tilde{N} \triangleq \dot{g}(p,\eta) - \dot{g}(p_d,\eta) + \alpha_1\left(r - \alpha_2 e_2 - \alpha_1 e_2 + \alpha_1^2 e_1\right) + \alpha_2 M\left(r - \alpha_2 e_2\right) + e_2 \quad (22)$$

$$N_d \triangleq -\ddot{p}_d + \dot{g}(p_d,\eta) \quad (23)$$

The motivation for defining the auxiliary functions in Eqn. (22) and Eqn. (23) is based on the fact that the following inequalities can be developed:

$$\| \tilde{N} \| \le \rho_0 \| z \|,\ \| N_d \| \le \zeta_{N_d},\ \| \dot{N}_d \| \le \zeta_{\dot{N}_d} \quad (24)$$

where $\rho_0,\ \zeta_{N_d},\ \zeta_{\dot{N}_d} \in \mathbb{R}^+$ are known bounding constants, and $z(t) \in \mathbb{R}^6$ is defined as

$$z \triangleq \begin{bmatrix} e_1^T & e_2^T & r^T \end{bmatrix}^T. \quad (25)$$

Based on the open loop error dynamics in Eqn. (21), the control input is designed via

$$\dot{u} = B^{-1}(-(k_s + I_{2\times 2})r - \beta sgn(e_2(t))) \quad (26)$$

where $k_s,\ \beta \in \mathbb{R}^{2\times 2}$ denote constant, positive definite, diagonal control gain matrices, and $I_{2\times 2}$ denotes a 2×2 identity matrix. Note that the control input $u(t)$ does not depend on the unmeasurable acceleration term $r(t)$, since Eqn. (26) can be directly integrated to show that $u(t)$ requires measurements of $e_1(t)$ and $e_2(t)$ only. To facilitate the following stability proof, the control gain matrix β in Eqn. (26) is selected to satisfy the sufficient condition

$$\lambda_{\min}(\beta) > \zeta_{N_d} + \frac{1}{\alpha_2}\zeta_{\dot{N}_d} \quad (27)$$

where $\lambda_{\min}(\cdot)$ denotes the minimum eigenvalue of the argument. After substituting Eqn. (26) into Eqn. (21), the closed-loop error dynamics are obtained as

$$M\dot{r} = \tilde{N} + N_d - (k_s + I_{n\times n})r + \beta sgn(e_2(t)) - e_2 \quad (28)$$

Theorem 0.1. The controller given in Eqn. (26) ensures asymptotic regulation of pitching and plunging displacements in the sense that

$$\|e_1(t)\| \to 0 \quad \text{as} \quad t \to \infty \tag{29}$$

provided the control gain k_s is selected sufficiently large, and β is selected according to the sufficient condition in Eqn. (27).

Lemma 0.2. To facilitate the following proof, let $\mathcal{D} \subset \mathbb{R}^7$ be a domain containing, $w(t) = 0$, where $w(t) \in \mathbb{R}^7$ is defined as

$$w(t) \triangleq \left[z^T \quad \sqrt{P(t)} \right]^T. \tag{30}$$

In Eqn. (30), the auxiliary function $P(t) \in \mathbb{R}$ is the generalized solution to the differential equation

$$\dot{P}(t) = -L(t) \tag{31}$$

$$P(0) = \beta \|e_2(0)\| - N_d^T(0) e_2(0) \tag{32}$$

where the auxiliary function $L(t) \in \mathbb{R}$ is defined as

$$L(t) = r^T \left(N_d(t) - \beta sgn(e_2) \right) \tag{33}$$

Provided the sufficient condition in Eqn. (27) is satisfied, the following inequality can be obtained:

$$\int_0^t L(\tau) d\tau \le \beta \|e_2(0)\| - N_d^T(0) e_2(0). \tag{34}$$

Hence, equation Eqn. (34) can be used to conclude that $P(t) \ge 0$.

Proof. (See Theorem 0.1) Let $V(w, t) : \mathcal{D} \times [0, \infty) \to \mathbb{R}$ be defined as the nonnegative function

$$V(w,t) \triangleq \tfrac{1}{2} e_1^T e_1 + \tfrac{1}{2} e_2^T e_2 + \tfrac{1}{2} r^T M r + P \tag{35}$$

where $e_1(t)$, $e_2(t)$, and $r(t)$ are defined in Eqn. (17), Eqn. (18) and Eqn. (19), respectively; and the positive definite function $P(t)$ is defined in Eqn. (31). The function $V(w, t)$ satisfies the inequality

$$U_1(w) \le V(w,t) \le U_2(w) \tag{36}$$

provided the sufficient condition introduced in Eqn. (27) is satisfied, where $U_1(w), U_2(w) \in \mathbb{R}$ denote the positive definite functions

$$U_1 \triangleq \lambda_1 \|w\|^2, \quad U_2 \triangleq \lambda_2 \|w\|^2 \tag{37}$$

where $\lambda_1 = \min\left\{\frac{1}{2}, \lambda_{\min}(M)\right\}$ and $\lambda_2 = \max\left\{1, \lambda_{\max}(M)\right\}$ After taking the time derivative of Eqn. (35) and utilizing Eqn. (18), as

$$\dot{V}(w,t) \le -(\alpha_1 - \tfrac{1}{2})\|e_1\|^2 - (\alpha_2 - \tfrac{1}{2})\|e_2\|^2 - \|r\|^2 - k_s \|r\|^2 + \rho_0 \|z\| \|r\| \tag{38}$$

where the bounds in Eqn. (24) were used, and the fact that eT1 $e_1^T e_2 \le \frac{1}{2}\|e_1\|^2 + \frac{1}{2}\|e_2\|^2$ (i.e., Young's inequality) was utilized. After completing the squares in Eqn. (38), the upper bound on $\dot{V}(w, t)$ can be expressed as,

$$\dot{V}(w,t) \le -(\alpha_1 - \tfrac{1}{2})\|e_1\|^2 - (\alpha_2 - \tfrac{1}{2})\|e_2\|^2 - \|r\|^2 - k_s \left(\|r\| - \frac{\rho_0}{2k_s} \|z\| \right)^2 + \frac{\rho_0^2}{4k_s} \|z\|^2. \tag{39}$$

Since $k_s > 0$, the upper bound in Eqn. (39) can be expressed as

$$\dot{V}(w,t) \le -\left(\lambda_0 - \frac{\rho_0^2}{4k_s} \right) \|z\|^2 \tag{40}$$

where $\lambda_0 \triangleq \min\{\alpha_1 - \frac{1}{2}, \alpha_2 - \frac{1}{2}, 1\}$. The following expression can be obtained from Eqn. (40):

$$\dot{V}(w, t) \le -U(w) \tag{41}$$

where $U(w) = c\|z\|^2$, for some positive constant $c \in \mathbb{R}$, is a continuous, positive semi-definite function.

It follows directly from the Lyapunov analysis that $e_1(t), e_2(t), r(t) \in \mathcal{L}_\infty$. This implies that $\dot{e}_1(t), \dot{e}_2(t) \in \mathcal{L}_\infty$ from the definitions given in Eqn. (18) and Eqn. (19). Given that $\dot{e}_1(t), e_2(t), r(t) \in \mathcal{L}_\infty$, it follows that $\ddot{e}_1(t) \in \mathcal{L}_\infty$ from Eqn. (19). Thus, Eqn. (17) can be used to prove that $p(t), \dot{p}(t), \ddot{p}(t) \in \mathcal{L}_\infty$. Since $p(t), \dot{p}(t), \ddot{p}(t) \in \mathcal{L}_\infty$, Eqn. (16) can be used to prove that $u(t) \in \mathcal{L}_\infty$. Since $r(t)$, $u(t) \in \mathcal{L}_\infty$, Eqn. (26) can be used to show that $\dot{u}(t) \in \mathcal{L}_\infty$. Given that $e_1(t), e_2(t), r(t), \dot{u}(t) \in \mathcal{L}_\infty$, Eqn. (28) can be used along with Eqn. (24) to prove that $\dot{r}(t) \in \mathcal{L}_\infty$ Since $\dot{e}_1(t), \dot{e}_2(t), \dot{r}(t) \in \mathcal{L}_\infty$, $e_1(t), e_2(t), r(t)$ are uniformly continuous. Equation (25) can then be used to show that $z(t)$ is uniformly continuous. Given that $e_1(t), e_2(t), r(t) \in \mathcal{L}_\infty$, Eqn. (35) and

Eqn. (40) can be used to prove that $z(t) \in \mathcal{L}_\infty \cap \mathcal{L}_2$ Barbalat's lemma [7] can now be invoked to prove that $\| z(t) \| \to 0$ as $t \to \infty$. Hence, $\|e_1(t)\| \to 0$ as $t \to \infty$ from Eqn. (25). Further, given that $V(w, t)$ in Eqn. (35) is radially unbounded, convergence of $e_1(t)$ is guaranteed regardless of initial conditions, which is a global result.

$\rho = 1.1 kg/m^3$	$b = 0.11\, m$	$a = -0.024\, m$
$m = 2.55\, kg$	$a_1 = 0.165$	$a_2 = 0.0455$
$S_\alpha = 1.04 \times 10^{-2}\, kg \cdot m$	$b_1 = 0.335$	$b_2 = 0.300$
$I_\alpha = 2.51 \times 10^{-3}\, kg \cdot m$	$k_\alpha = 9.3\, N/m$	$k_{\alpha^3} = 55\, N/m$
$k_h = 450\, N/m$	$\zeta_h = 5.5 \times 10^{-3}$	$\zeta_\alpha = 1.8 \times 10^{-2}$

Table 1. Parameters of aeroelastic model.

3 Results

In the current study, a representative set of the aeroelastic model's parameters shown in Table 1 is selected to provide a realistic model of the elastically-mounted wing section. The structural parameters were previously employed in Ref. [2] to match with experimental study in Ref. [8] which indicated a critical (flutter) speed of about 16 m/s in this test case. Fig. 2 from Ref. [2] shows comparison of the pitching LCO amplitudes obtained from the 2-DOF quasilinear aeroelastic model (Section 2) against numerical and experimental results of Ref. [8].

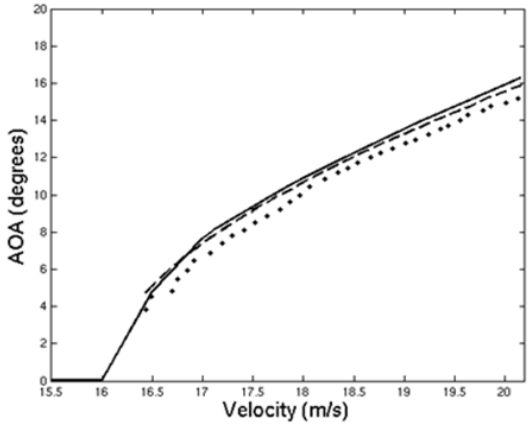

Fig. 2. Flat-plate pitching LCO amplitudes: current quasilinear aeroelastic model predictions (solid line) vs. numerical analysis (dashed line) and experiment (markers) of Ref. [8].

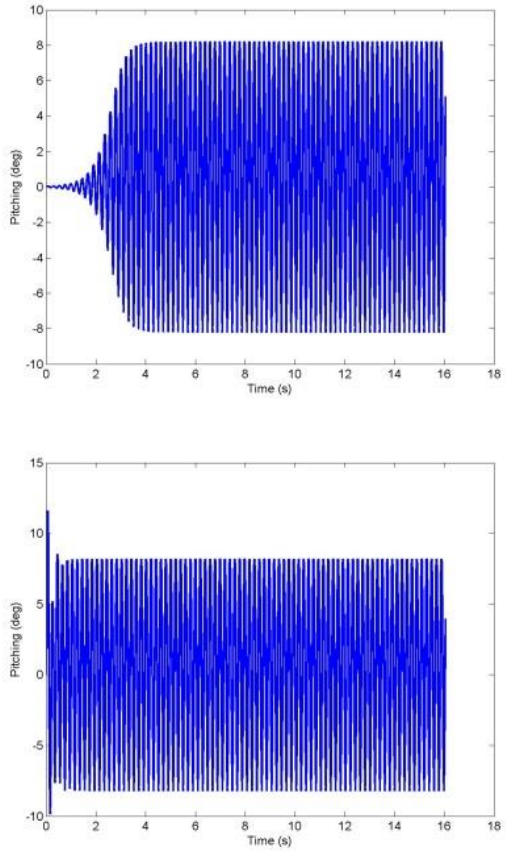

Fig. 3. Transition to uncontrolled pitching LCO for increasing (top to bottom) amplitudes of initial excitation.

To demonstrate the performance of the robust control law developed in Section 2.1, several test cases have been performed. Fig. 3 first illustrates results of the reduced-order simulations for uncontrolled 2-DOF flat-plate pitching LCO obtained for the flow speed of 19 m/s for two initial airfoil excitation amplitudes corresponding to $\varepsilon_l = \dot{p}(0) =$ (0.002, 0.005) and $\varepsilon_h = \dot{p}(0) =$ (1, 2) (the state vector $p(t)$ is defined in Eqn. (2)). Cleary, the final LCO amplitudes are the same in both cases but the transition process is different. The plunging LCO characteristics have very similar features and thus are not shown.

The required control authority of the actuators changes correspondingly depending on the initial excitation and the LCO amplitudes (i.e., the flow speed, as shown in Fig. 2). Test computations are performed for the following selection of the control gains in the robust controller model:

$$\alpha_1 = \begin{bmatrix} 1 & 0 \\ 0 & 35 \end{bmatrix}, \quad \alpha_2 = \begin{bmatrix} 1 & 0 \\ 0 & 35 \end{bmatrix}, \quad k_s = \begin{bmatrix} 10^{-7} & 0 \\ 0 & 9\times10^{-4} \end{bmatrix}, \quad \beta = \begin{bmatrix} 10^{-3} & 0 \\ 0 & 25 \end{bmatrix} \tag{42}$$

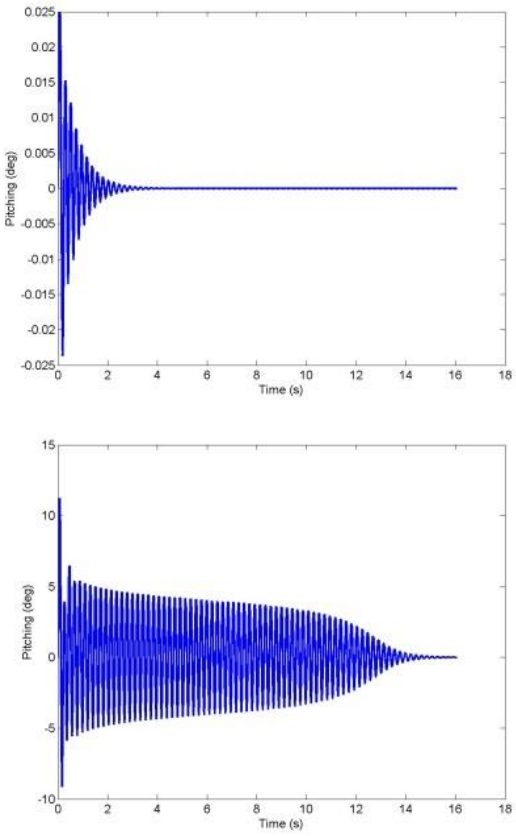

Fig. 4. Suppression of pitching LCO achieved by the feedback-loop robust control system with increasing (top to bottom) amplitudes of initial excitation.

Successful suppression of the pitching LCO is demonstrated for the three initial excitation amplitudes in Fig. 4, whereas the corresponding time histories of the aerodynamic lift and moment produced by the actuator governed by the robust controller are shown in Figs. 5-6. As expected, both the time required to suppress LCO oscillations and the amplitudes of the forces and moments to be delivered by the actuator operating in the feedback-loop robust control system increase with higher initial excitation amplitudes. Similarly, the control authority requirements become more demanding at higher supercritical flight speeds, and generally new optimized sets of control gains should be determined.

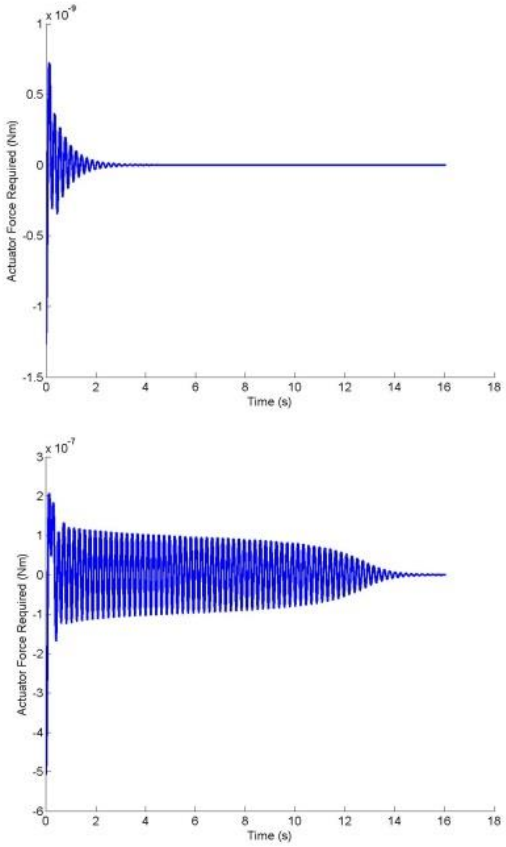

Fig. 5. Actuator's control authority requirements for aerodynamic lift with increasing (top to bottom) amplitudes of initial excitation.

4 Conclusions

The current work employed a reduced-order model to evaluate possible use of the synthetic-jet actuators as part of UAV robust, nonlinear feedback-loop flight control technology. A benchmark case of the robust control of 2-DOF airfoil gust-induced limit-cycle oscillations was considered. A rigorous mathematical analysis of the controller performance was performed addressing parametric uncertainty and nonlinearities inherent both in the upstream flow conditions and SJA dynamics. The proposed controller design is easily and inexpensively implementable, requiring no observers, function approximators, or adaptive update laws which would be required in alternative methods. Minimal knowledge of the structure of the SJA dynamic model is exploited, with matrix decomposition technique utilized along with innovative algebraic

manipulation in the control development to compensate for any dynamic uncertainties. Preliminary results of the low-fidelity modeling of LCO robust control were demonstrated to explore the effect of the upstream disturbance amplitude on the actuator's required control authority, with results of the high-fidelity studies to appear in the subsequent work.

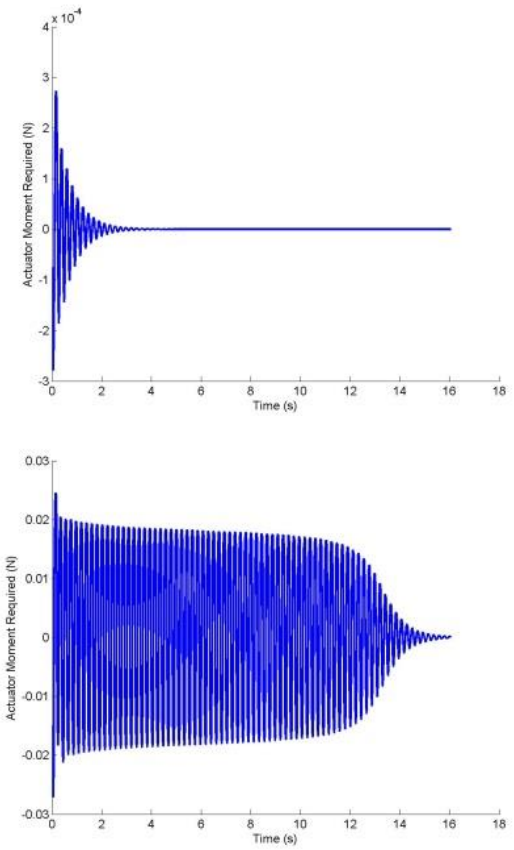

Fig. 6. Actuator's control authority requirements for aerodynamic moment with increasing (top to bottom) amplitudes of initial excitation.

Acknowledgement

The authors would like to acknowledge support for this work from the National Science Foundation (Award Number IIP-1346332, Program Director Dr. M.S. Nair).

References

[1] Golubev, V. V., and Visbal, M. R., Modeling MAV Response in Gusty Urban Environment. *International Journal of Micro Air Vehicles*, Vol. 4, pp. 79–92, 2012.

[2] Golubev, V. V., Dreyer, B. D., Hollensahde, T. M., and Visbal, M. R., High-Accuracy Viscous Simulation of Gust-Airfoil Nonlinear Aeroelastic Interaction. *AIAA Paper* 2009-4200, 2009.

[3] Golubev, V.V., and Nakhla, H., Modeling Synthetic Jets for Low-Re Airfoil Unsteady Flow Control. *International Journal of Emerging Multidisciplinary Fluid Sciences*, Vol. 3, pp. 145-158, 2012.

[4] O'Neil, T.O. and Strganac, T.W., Aeroelastic Response of a Rigid Wing Supported by Nonlinear Springs. *Journal of Aircraft*, Vol.35, No.4, pp. 616-622, 1998.

[5] Strganac, T.W. and Mook, D., Numerical Model of Unsteady Subsonic Aeroelastic Behavior. *AIAA Journal*, Vol. 28, No.5, pp. 903-909, 1990.

[6] Bisplinghoff, R.L., Ashley, H. and Halfman, R.L., Aeroelasticity. *Addison-Wesley*, 1957.

[7] Khalil, H. K., Nonlinear Systems. Vol. 3rd, *Prentice Hall*, 2001.

[8] Berggren, D., Investigation of Limit Cycle Oscillations for a Wing Section with Nonlinear Stiffness. *Aerospace Science and Technology*, Vol.8, pp. 27-34, 2004.

Contact Author Email Address

Vladimir.Golubev@erau.edu

Copyright Statement